The University of Reading

Lagrange-Remap Methods for the Euler Equations for Single and Multi Gas Flows

D.A. Bailey

3rd March 2003

Numerical Analysis Report 01/03

DEPARTMENT OF MATHEMATICS

Abstract

A solution method for the computation of steady Euler flows in one-dimension is presented. The approach is to combine the solution of the governing equations in a Lagrangian reference frame with an algorithm to remap the computational mesh. The aim is to retain the accuracy inherent with Lagrangian schemes and to av

Acknowledgments

I would like to thank my supervisors Dr. P.K. Sweby and Dr. P. Glaister (University of Reading Mathematics Departmen

Contents

1 Introduction

The Euler equations for one-dimensional unsteady compressible flow, in the reference frame of a moving control volume, can be expressed in integral form as

$$\frac{\partial}{\partial \mathrm{t}} \int_{\Omega(}$$

Lagrangian phase can then be considered as a solution for the sound wave related transport, and the rezoning of the grid can be viewed as the solution for the adv

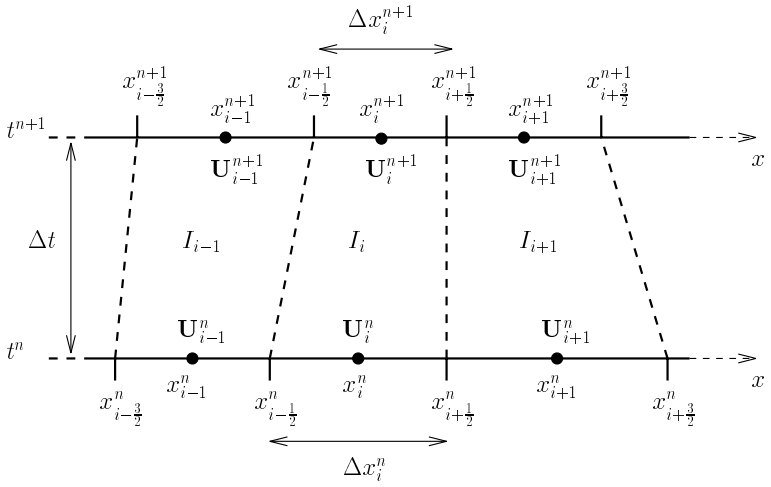

Figure 1: $x-t$ diagram of the computational mesh

In order to preserve conservation, the volume for cell I_i is updated by discretising the one-dimensional geometric conservation law (GCL)

$$\frac{\partial \Omega_i}{\partial \mathrm{t}} - \int_{\Gamma_i(t)} \dot{x}.\hat{n} \; \mathrm{d}\Gamma \; = \; 0 \tag{8}$$

in the following manner

$$\frac{\Omega_i^{n\ 1} - \Omega_i^n}{\Delta t} \quad = \quad -\dot{x}_{i-\frac{1}{2}} + \dot{x}_{i\ \frac{1}{2}} \, . \tag{9}$$

Here $\dot{x}_{i-\frac{1}{2}}$ is the grid velocity normal to the boundary $x_{i-\frac{1}{2}}$. Therefore, since $\dot{x} = u$ (Lagrangian reference frame), the volume is explicit

Time integration of particle position x_i is performed according to an estimate of the displacement of the centre of volume of cell I_i,

$$x_i^{n\ 1} = \frac{1}{\Omega_i^n + \Delta\Omega_i} \left(x_i^n \Omega_i^n + \left(g_{i-\frac{1}{2}} z_{i-\frac{1}{2}} + g_{i\ \frac{1}{2}} z_{i\ \frac{1}{2}} \right) \right) , \tag{12}$$

where $z_{i-\frac{1}{2}} = \hat{u}_{i-\frac{1}{2}} \Delta t$ is the additional cell volume created by normal displacement of the boundary $x^n_{i-\frac{1}{2}}$, ($\hat{u}_{i-\frac{1}{2}}$ is the outward normal velocity to the boundary $x^n_{i-\frac{1}{2}}$), $g_{i-\frac{1}{2}} = (x^n_{i-\frac{1}{2}} + u_{i-\frac{1}{2}} \Delta t/2)$ is the position of the centre of $z_{i-\frac{1}{2}}$, and $\Delta\Omega_i = \sum_{j=0}^{1} z_{i-\frac{1}{2}\ j}$ is the total change in cell I_i volume over time interval Δt [1].

This calculation can be viewed as a weighted av

Here $u_i^n = 0$ and the sound speed is the only contribution to $S_{\max}^n$. Underestimating the value of $S_{\max}^n$ results in a choice of Δt that is too large and instabilities may develop from the beginning of the computations. To circumvent this problem the C_{cfl} constant in (13) is reduced to 0.1 for the

The cell particles and their movements are indicated by the lines $A-A$ and $C-C$. The interface between the two relevant cells, which by definition is the contact wave of the Riemann problem, has position through time indicated by the line $B-B$. The $*$ superscript denotes the wave-processed states i.e the data states that are created due to the passage of three waves emerging from the origin of the initial discontinuity. S_L, S^*, and S_R are respectively the speed estimates for the left, contact and right waves.

It is required to calculate a numerical flux across the line $B-B$, that is across the cell interface, over time interval Δt.

Applying conservation of $\mathbf{U}$ on $A-B$ over the time interval Δt gives

$$\left.\frac{\Delta x}{2} - u_L\Delta t + S_L\Delta t\right)\mathbf{U}_L + (-b_L\Delta t) + \Delta t S^*\mathbf{U}_L^* \tag{15}$$

$$= \quad \frac{\Delta x}{2}\mathbf{U}_L + \Delta t\mathbf{F}_L - \Delta t\mathbf{F}_L^*$$

$$\Rightarrow \quad (S_L - u_L)\,\mathbf{U}_L + (S^* - S_L)\,\mathbf{U}_L^* = \mathbf{F}_L - \mathbf{F}_L^* \tag{16}$$

$$\Rightarrow \quad \mathbf{F}_L^* + (S^* - S_L)\,\mathbf{U}_L^* = \mathbf{F}_L + (u_L - S_L)\,\mathbf{U}_L \tag{17}$$

$$\Rightarrow \quad \mathbf{F}_L^* = \mathbf{F}_L + \mathbf{U}_L^*\left(S^L - S_*\right) - \mathbf{U}_L\left(S_L - u_L\right) \tag{18}$$

Similarly, conservation of $\mathbf{U}$ on $B-C$ over the time interval Δt yields

$$\mathbf{F}_R^* + (S^* - S_R)\,\mathbf{U}_R^* = \mathbf{F}_R + (u_R - S_R)\,\mathbf{U}_R \tag{19}$$

$$\Rightarrow \quad \mathbf{F}_R^* = \mathbf{F}_R + \mathbf{U}_R^*\left(S^R - S_*\right) - \mathbf{U}_R\left(S_R - u_R\right) \tag{20}$$

The wave processed states and the corresponding lagrangian fluxes take the form

$$\mathbf{U}_K^* = \begin{pmatrix} \rho_K^* \\ \rho_K^* u_K^* \\ \rho_K^* \quad {}_K^* \end{pmatrix} \quad \text{and} \quad \mathbf{F}_K^* = \begin{pmatrix} 0 \\ p_K^* \\ u_K^* p_K^* \end{pmatrix}, \tag{21}$$

where $K = L, R$ and $S^* = u_L^* = u_R^* = u^* = u_{i\ \frac{1}{2}}$ is an approximation of the fluid velocity normal to the boundary $x_{i\ \frac{1}{2}}$. Therefore, by substitution of these quantities into (17) and (19), and by consideration of the individual rows of these vector equations, it can be shown that

$$\rho_K^* = \rho_K\frac{(S_K - u_K)}{(S_K - S^*)}, \tag{22}$$

$$\rho_K^* u_K^* = \rho_K\frac{(S_K - u_K)}{(S_K - S^*)}S^*, \tag{23}$$

$$p_K^* = p_K + \rho_K\,(u_K - S_K)\,(u_K - S^*)\,, \tag{24}$$

and

$$\rho_K^* \quad {}_K^* = \rho_K \frac{(S_L - u_L)}{(S_L - S^*)} \left[\quad {}_K + (S^* - u_K) \quad S^* + \frac{p_K}{\rho_K (S_K - u_K)} \right) \right] , \qquad (25)$$

for $K = L, R$. The intercell numerical flux is then calculated via averaging of equations (18) and (20)

$$\mathbf{F}_{i \ \frac{1}{2}} = \left(\mathbf{F}_L^* + \mathbf{F}_R^* \right) / 2 \, , \qquad (26)$$

where the $\mathbf{U}_K^*$, $K = L, R$, vector in (18) and (20) are obtained using equations (22), (23) and (25).

Following the original approach suggested by Toro et. al. [12], the wave speed estimates, S_L, S^*andS_R, are acquired from

$$S_L = u_L - a_L q_L \, , \qquad S^* = u^* \, , \quad S_R = u_R + a_R q_R \, , \qquad (27)$$

where a_L, a_R are the local sound speeds in the undisturbed fluid, and q_K, for $K = L, R$, is a parameter defined by

$$q_K = \begin{cases} 1 & H_K \leq 1 \\ \sqrt{1 + \frac{\gamma \ 1}{2\gamma} (H_K - 1)} & \text{otherwise} \end{cases} . \qquad (28)$$

Here $H_K = \tilde{p}^* / p_K$, and $\tilde{p}^*$ and u^* are estimates for the wave processed presure and velocity. If the K wave is a rarefraction then the speed S_K corresponds to the characteristic speed of the head of the rarefraction. If the wave is a shock then S_K corresponds to an approximation to the true shock speed; the wave relations used are exact but the pressure ratio across the discontinuity is approximated, because the value of $\tilde{p}^*$ is an estimate.

In this work, values for $\tilde{p}^*$ and u^* are calculated using the adaptive/hybrid approach proposed by Toro [12], which is based on his exact Riemann solver. The method is described algorithmically below:

- The initial approximation for the pressure is evaluated using

$$\tilde{p}_{\text{int}}^* = \frac{1}{2} (p_L + p_R) - \frac{1}{2} (u_L - u_R) \, \overline{\rho} \, \overline{a} \, , \qquad (29)$$

  where $\overline{a} = (a_L + a_R)/2$ and $\overline{\rho}$ ximated/TD1TD1ximation/n1//TD1RTj1/TJ11LTj1T

- If $\tilde{p}^*_{\text{int}} < p_{\min}$, suggesting that the 2 non-linear waves in the exact solution to the Riemann problem are rarefraction waves, then

$$\tilde{p}^* = \left[\frac{a_L + a_R - \frac{\gamma-1}{2}(u_R - u_L)}{\frac{a_L}{p_L^z} + \frac{a_R}{p_R^z}} \right]^{\frac{1}{z}}, \tag{32}$$

$$u^* = u_L - \frac{2a_L}{(\gamma-1)} \left[\left(\frac{\tilde{p}^*}{p_L} \right)^z - 1 \right]. \tag{33}$$

  where $z = \frac{\gamma-1}{2\gamma}$.

- Else the 2 non-linear waves in the exact solution of the Riemann problem are assumed to be shock waves, and

$$\tilde{p}^* = \frac{g_L(p_0)\, p_L + g_R(p_0)\, p_R - (u_R - u_L)}{g_L(p_0) + g_R(p_0)}, \tag{34}$$

$$u^* = \frac{1}{2}(u_L + u_R) + \frac{1}{2}\left[(\tilde{p}^* - p_R)\, g_R(p_0) - (\tilde{p}^* - p_L)\, g_L(p_0) \right], \tag{35}$$

  where

$$g_K(p) = \left[\frac{A_K}{p + B_K} \right]^{\frac{1}{2}}, \tag{36}$$

$$A_K = \frac{2}{(\gamma+1)\,\rho_K}, \tag{37}$$

$$B_K = \frac{(\gamma-1)}{(\gamma+1)} p_K, \qquad K = L, R, \tag{38}$$

  and

$$p_0 = \max(0, \tilde{p}^*_{\text{int}}). \tag{39}$$

The initial appro

Second Order Accuracy For HLLC

In this work, second order accuracy for the Lagrangian HLLC Riemann solver is achieved using the MUSCL-Hancock approach [12]. The method can be divided into 3 stages:

Stage 1: Data Reconstruction

The piecewise constant data cell average values $\mathbf{U}_i^n$ are locally replaced by piecewise linear functions in each cell $[x_{i-\frac{1}{2}}, x_{i\ \frac{1}{2}}]$ according to

$$\mathbf{U}_i^n(x) = \mathbf{U}_i^n + (x - x_i)\,\tilde{\sigma}_i\,, \qquad x \in [x_{i-\frac{1}{2}}, x_{i\ \frac{1}{2}}]\,, \tag{40}$$

where $\tilde{\sigma}_i$ is a vector of limited first derivative approximations. The values of $\mathbf{U}_i^n(x)$ at the cell boundaries of cell I_i are

$$\mathbf{U}_i^L = \mathbf{U}_i^n - \frac{\Delta x_i}{2}\tilde{\sigma}_i \quad \text{and} \tag{41}$$

$$\mathbf{U}_i^R = \mathbf{U}_i^n + \frac{\Delta x_i}{2}\tilde{\sigma}_i\,, \tag{42}$$

and are called boundary extrapolated values.

The two alternative methods used in this work for evaluating the vector $\tilde{\sigma}_i$ are described in detail in the next subsection.

Stage 2: Evolution

The boundary extrapolated values $\mathbf{U}_i^L$ and $\mathbf{U}_i^R$ are considered to be cell average values, and are evolved by $\frac{1}{2}\Delta t$ using a conservative scheme in which the numerical flux is equal to the exact flux function evaluated at the extrapolated values. That is,

$$\overline{\mathbf{U}}_i^L = \mathbf{U}_i^L + \frac{1}{2}\frac{\Delta t}{\Delta x_i^n}\left[\mathbf{F}\left(\mathbf{U}_i^L\right) - \mathbf{F}\left(\mathbf{U}_i^R\right)\right]\,, \tag{43//TD1i//TD1i/w}$$

R
i= U

U

Wave-By-Wave Slope Limiting.

The vector $\tilde{\sigma}_i$ in cell I_i is taken to be a function of the derivatives $\left(\frac{\Delta_{i-\frac{1}{2}}}{\Delta x_{i-\frac{1}{2}}}\right.$ and $\left.\frac{\Delta_{i+\frac{1}{2}}}{\Delta x_{i+\frac{1}{2}}}\right)$, namely

$$\tilde{\sigma}_i = \tilde{\sigma}_i \left(\frac{\Delta_{i-\frac{1}{2}}}{\Delta x_{i-\frac{1}{2}}}, \frac{\Delta_{i\ \frac{1}{2}}}{\Delta x_{i\ \frac{1}{2}}} \right) , \tag{50}$$

where

$$\Delta_{i-\frac{1}{2}} = \mathbf{U}_i^n - \mathbf{U}_{i-1}^n \quad ; \quad \Delta_{i\ \frac{1}{2}} = \mathbf{U}_{i\ 1}^n - \mathbf{U}_i^n ; \tag{51}$$

$$\Delta x_{i-\frac{1}{2}} = x_i - x_{i-1} \quad ; \quad \Delta x_{i\ \frac{1}{2}} = x_{i\ 1} - x_i . \tag{52}$$

The arguments $\Delta_{i-\frac{1}{2}}$

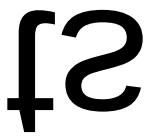

thus, allowing the limiting process to be applied wave-by-wave.

The limited derivatives are evaluated component-wise using

$$\tilde{\sigma}_i^{(m)}\left(\frac{\Delta^{(m)}_{i-\frac{1}{2}}}{\Delta x_{i-\frac{1}{2}}},\frac{\Delta^{(m)}_{i\ \frac{1}{2}}}{\Delta x_{i\ \frac{1}{2}}}\right) = \begin{cases} \max\left[0,\min\left(\frac{\beta\Delta^{(m)}_{i-\frac{1}{2}}}{\Delta x_{i-\frac{1}{2}}},\frac{\Delta^{(m)}_{i+\frac{1}{2}}}{\Delta x_{i+\frac{1}{2}}}\right),\min\left(\frac{\Delta^{(m)}_{i-\frac{1}{2}}}{\Delta x_{i-\frac{1}{2}}},\frac{\beta\Delta^{(m)}_{i+\frac{1}{2}}}{\Delta x_{i+\frac{1}{2}}}\right)\right] & \Delta^{(m)}_{i\ \frac{1}{2}} \geq 0 \\ \min\left[0,\max\left(\frac{\beta\Delta^{(m)}_{i-\frac{1}{2}}}{\Delta x_{i-\frac{1}{2}}},\frac{\Delta^{(m)}_{i+\frac{1}{2}}}{\Delta x_{i+\frac{1}{2}}}\right),\max\left(\frac{\Delta^{(m)}_{i-\frac{1}{2}}}{\Delta x_{i-\frac{1}{2}}},\frac{\beta\Delta^{(m)}_{i+\frac{1}{2}}}{\Delta x_{i+\frac{1}{2}}}\right)\right] & \Delta^{(m)}_{i\ \frac{1}{2}} \leq 0 \end{cases} \quad (55)$$

where the value $\beta = 1$ reproduces a minmod-type limiter, and $\beta = 2$ reproduces a superbee-type limiter.

Equation (55) has been established by forcing equivalence of MUSCL-type schemes with conventional flux limiter methods, for the model scalar equation on a fixed Eulerian grid [12]. The result then being modified to allow for the varying cell volumes associated with Lagrangian methods.

4 The Roe Solver

The Roe solver calculates a numerical approximation to the solution of hyperbolic conservation laws by solving a constant coefficient [illegible]

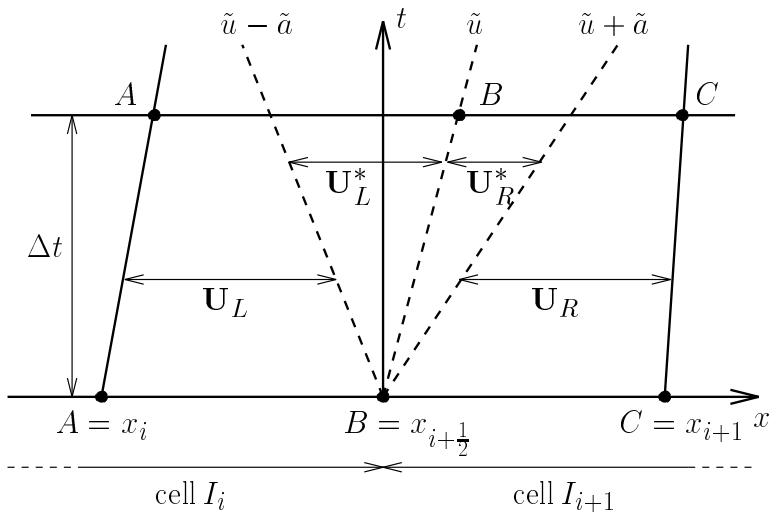

Figure 4: Schematic of approximate Riemann solution in Lagrangian control volume ABC.

For a fixed grid, diagonalising the Roe linearisation for the system of non-linear equations allows the flux between the two adjacent cells I_i and $I_{i\ 1}$ (i.e the flux across the t-axis) to be written as

$$\mathbf{F}_{i\ \frac{1}{2}}(\mathbf{U}_L,\mathbf{U}_R)=\frac{1}{2}\left[\mathbf{F}_L(\mathbf{U}_L)+\mathbf{F}_R(\mathbf{U}_R)-\sum_{m=1}^{3}\tilde{\alpha}_{i\ \frac{1}{2}}^{(m)}|\tilde{\lambda}_{\text{adv}}^{(m)}+\tilde{\lambda}_{\text{rel}}^{(m)}|\tilde{\mathbf{e}}_{i\ \frac{1}{2}}^{(m)}\right], \tag{56}$$

where

$$\mathbf{F}_K(\mathbf{U}_K)=u_K\mathbf{U}_K+\begin{pmatrix}0\\ p_K\\ u_Kp_K\end{pmatrix}, \quad K=L,R, \tag{57}$$

the wave strengths are given by

$$\tilde{\alpha}_{i\ \frac{1}{2}}^{(1)} = \frac{1}{2\tilde{a}}\left[(\rho_R-\rho_L)(\tilde{u}+\tilde{a})-(\rho_Ru_R-\rho_Lu_L)-\tilde{a}\tilde{\alpha}^{(2)}\right], \tag{58}$$

$$\tilde{\alpha}_{i\ \frac{1}{2}}^{(2)} = \frac{\gamma-1}{\tilde{a}^2}\Big[(\rho_R-\rho_L)\left(\tilde{H}-\tilde{u}^2\right)+\tilde{u}(\rho_Ru_R-\rho_Lu_L)- (\rho_R\ \ _R-\rho_L\ \ _L)\Big], \tag{59}$$

$$\tilde{\alpha}_{i\ \frac{1}{2}}^{(3)} = (\rho_R-\rho_L)-\left(\tilde{\alpha}^{(1)}+\tilde{\alpha}^{(2)}\right), \tag{60}$$

the eigenvalues are

$$\tilde{\lambda}^{(1)}_{\rm adv} = \tilde{u} \qquad , \qquad \tilde{\lambda}^{(1)}_{\rm rel} = -\tilde{a}\,, \tag{61}$$

$$\tilde{\lambda}^{(2)}_{\rm adv} = \tilde{u} \qquad , \qquad \tilde{\lambda}^{(2)}_{\rm rel} = 0\,, \tag{62}$$

$$\tilde{\lambda}^{(3)}_{\rm adv} = \tilde{u} \qquad , \qquad \tilde{\lambda}^{(3)}_{\rm rel} = \tilde{a}\,, \tag{63}$$

and the corresponding right eigenvectors are

$$\tilde{\mathbf{e}}^{(1)}_{i\ \frac{1}{2}} = \begin{pmatrix} 1 \\ \tilde{u} - \tilde{a} \\ \tilde{H} - \tilde{u}\tilde{a} \end{pmatrix}, \quad \tilde{\mathbf{e}}^{(2)}_{i\ \frac{1}{2}} = \begin{pmatrix} 1 \\ \tilde{u} \\ \frac{1}{2}\tilde{u}^2 \end{pmatrix}, \quad \tilde{\mathbf{e}}^{(3)}_{i\ \frac{1}{2}} = \begin{pmatrix} 1 \\ \tilde{u} + \tilde{a} \\ \tilde{H} + \tilde{u}\tilde{a} \end{pmatrix}. \tag{64}$$

Here, $\tilde{u} = u_{i\ \frac{1}{2}}$ is an approximation of the fluid velocity normal to the boundary $x_{i\ \frac{1}{2}}$, and

$$\tilde{u} = \frac{\sqrt{\rho_L}u_L + \sqrt{\rho_R}u_R}{\sqrt{\rho_L} + \sqrt{\rho_R}} \tag{65}$$

$$\tilde{H} = \frac{\sqrt{\rho_L}H_L + \sqrt{\rho_R}H_R}{\sqrt{\rho_L} + \sqrt{\rho_R}} \tag{66}$$

$$\tilde{a}^2 = (\gamma - 1)\left[\tilde{H} - \frac{1}{2}\tilde{u}^2\right]. \tag{67}$$

Here H_K, $K = L, R$, is the total enthalpy

$$H_K = \frac{_K + p_K}{\rho_K} \qquad K = L, R\,. \tag{68}$$

The tilde is used to indicate a Roe averaged value.

The flux function (56) has been written in such a way that its value, the flux relative to a fixed grid, can be split naturately into two quantities; the flux which is a result of advection with the flow; and the flux relative to the flow.

Therefore, to determine the flux between the two cells I_i and $I_{i\ 1}$ in a Lagrangian frame of reference (i.e. the flux across the $B - B$ in Figure 4), one simply subtracts the flux resulting from advection with the flow from equation (56)

$$\mathbf{F}_{i\ \frac{1}{2}}(\mathbf{U}_L, \mathbf{U}_R) = \frac{1}{2}\left[\mathbf{F}_L(\mathbf{U}_L) + \mathbf{F}_R(\mathbf{U}_R) - \sum_{m=1}^{3} \tilde{\alpha}^{(m)}_{i\ \frac{1}{2}} |\tilde{\lambda}^{(m)}_{\rm rel}| \{\pm\right.$$

and the remaining variables are given by equations (58) to (67).

It is well known that Roe's scheme for the Euler equations on a fixed grid permits non-physical stationary discontinuities; a sonic expansion wave may be incorrectly approximated by a rarefraction shock. Hence, Roe's approximate Riemann Solver in general does not satisfy an entropy inequality. However, it can be modified to eliminate these entropy violating discontinuities while retaining those that satisfy the entropy law. Such an entropy fix is not necessary in the Lagrangian case, because shock and expansion waves move with respect to the Lagrangian reference frame [15].

Second-Order Accuracy For Roe

In this work, second-order accuracy for the Lagrangian Roe solver is achieved using flux limiting. The method is to linearize the system of non-linear equations using Roe's approximate Riemann solver, diagonalise, and then apply flux-limiting to each of the resulting scalar equations [4].

Taking Godunov's scheme to calculate the first-order flux and the Lax-Wendroff scheme to evaluate the second-order flux, the numerical flux between cell I_i and $I_{i\ 1}$, for the corresponding fixed grid flux-limiter solver, can be written as

$$\mathbf{F}_{i\ \frac{1}{2}}(\mathbf{U}_L, \mathbf{U}_R) = \frac{1}{2}\Bigg[\mathbf{F}_L(\mathbf{U}_L) + \mathbf{F}_R(\mathbf{U}_R) - \sum_{m=1}^{3}\Bigg\{\Bigg[1 - \phi.\Bigg(1 - \frac{\Delta t}{\Delta x_{i\ \frac{1}{2}}}|\tilde{\lambda}^{(m)}_{\mathrm{adv}} + \tilde{\lambda}^{(}$$

- the minbee limiter:

$$\phi(r) = \begin{cases} 0 & r \leq 0 \\ r & 0 \leq r \leq 1 \\ 1 & r \geq 1 \end{cases} , \tag{73}$$

- the van Leer limiter:

$$\phi(r) = \begin{array}{ll} 0 & r \leq 0 \\ \frac{2r}{1\ r} & r \geq 0 \end{array} , \tag{74}$$

- the superbee limiter:

$$\phi(r) = \begin{cases} 0 & r \leq 0 \\ 2r & 0 \leq r \leq \frac{1}{2} \\ 1 & \frac{1}{2} \geq 1 \\ r & 1 \leq r \leq 2 \\ 2 & r \geq 2 \end{cases} . \tag{75}$$

Subtraction of the flux resulting from advection with the flow from equation (71) produces the required second-order accurate Lagrangian flux

$$\begin{aligned} \mathbf{F}_{i\ \frac{1}{2}}(\mathbf{U}_L, \mathbf{U}_R) \;=\; & \frac{1}{2}\Bigg[\mathbf{F}_L(\mathbf{U}_L) + \mathbf{F}_R(\mathbf{U}_R) - \\ & \sum_{m=1}^{3} \Bigg\{ \left[1 - \phi. \left(1 - \frac{\Delta t}{\Delta x_{i\ \frac{1}{2}}} |\tilde{\lambda}^{(m)}_{\mathrm{rel}}| \right) \right] \\ & .|\tilde{\lambda}^{(m)}_{\mathrm{rel}}|\, \tilde{\alpha}^{(m)}_{i\ \frac{1}{2}}\, \tilde{\mathbf{e}}^{(m)}_{i\ \frac{1}{2}} \Bigg\} \Bigg] , \end{aligned} \tag{76}$$

where $\mathbf{F}_L, \mathbf{F}_R$ are given by equation (70), $\phi = \phi(r)$ with

$$r = \frac{\tilde{\alpha}^{(m)}_{i'}}{\tilde{\alpha}^{(m)}_{i\ \frac{1}{2}}} \qquad \text{and} \qquad i' = i + \frac{1}{2} + \mathrm{sign}\left(\tilde{\lambda}^{(m)}_{\mathrm{rel}}\right) , \tag{77}$$

and the remaining variables are given by equations (58) to (67) and (73) to (75).

5 Rezoning

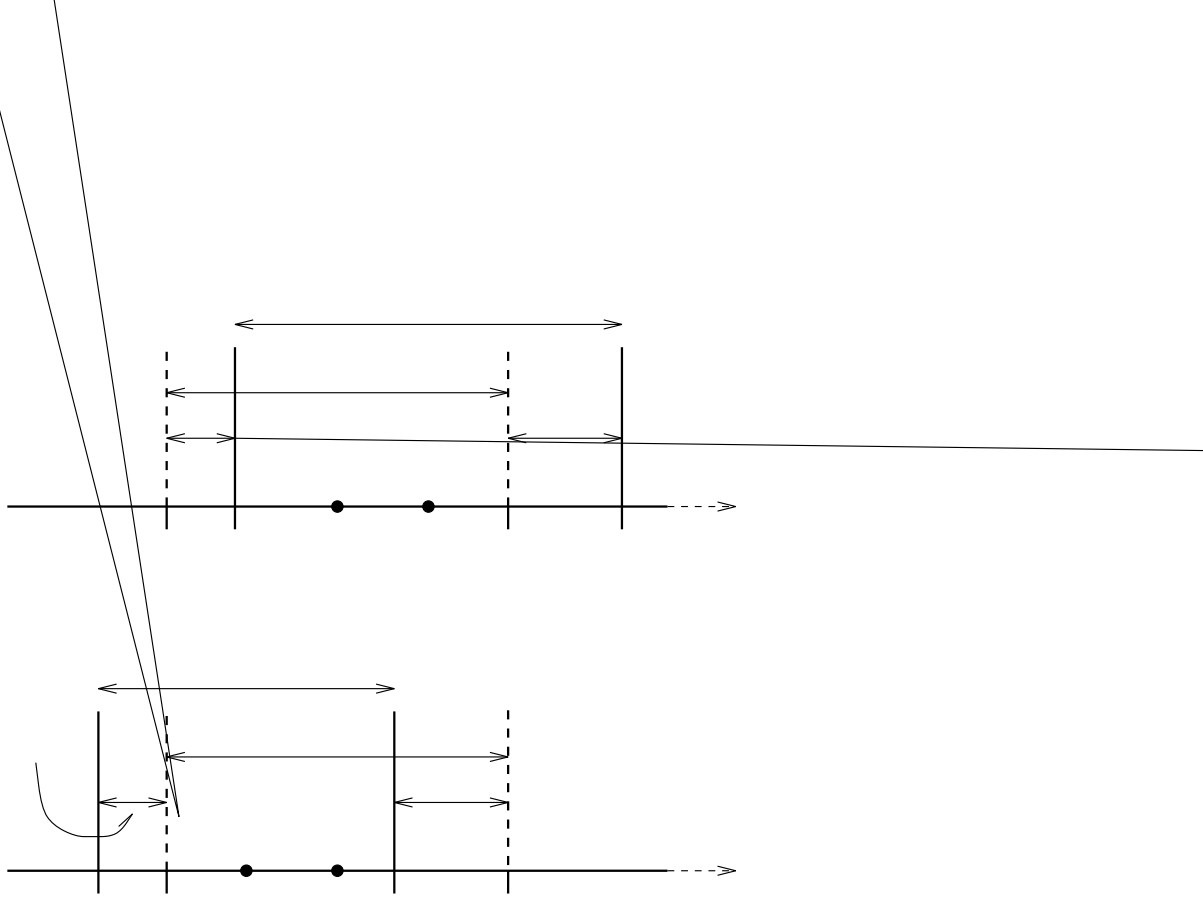

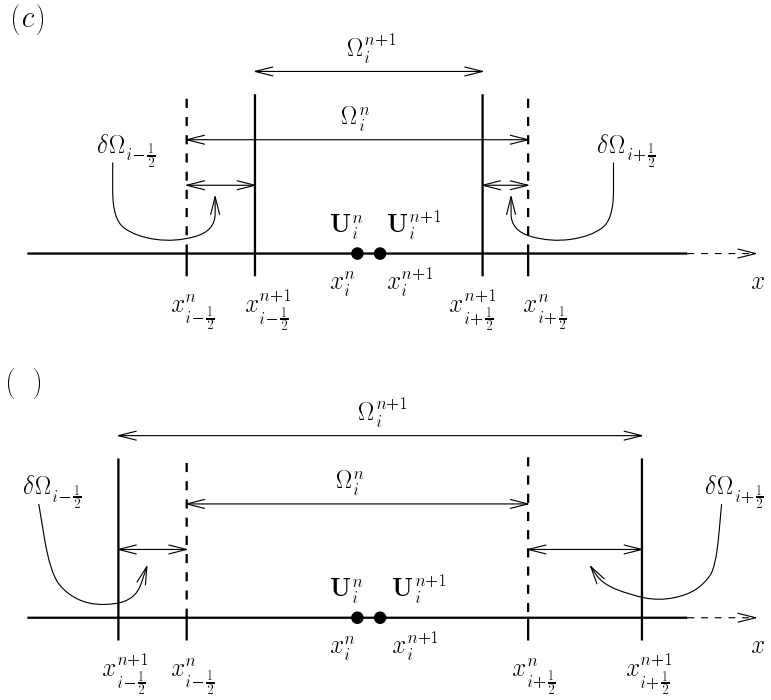

Figure 6: $x-U$ diagrams for cell I_i of cell contraction and expansion resulting from the Lagrangian phase.

$\dot{x}_{i-\frac{1}{2}}$ and are dependent on the type of data reconstruction applied in each cell.

As discussed earlier, the rezoning phase can be viewed as an advection process. Interpreting equation (81) in this way, the quantity $\delta\Omega_{i-\frac{1}{2}}$ can be seen as a volume flux, and the components of the vector $\hat{\mathbf{F}}_{i-\frac{1}{2}}$ can be viewed as advection fluxes divided by the velocity normal to the corresponding boundary. That is

$$\hat{\mathbf{F}}_{i-\frac{1}{2}} = \frac{\mathbf{F}_{i-\frac{1}{2}}}{\dot{x}_{i-\frac{1}{2}}}, \tag{83}$$

where $\mathbf{F}_{i-\frac{1}{2}}$ is a vector of numerical advection fluxes which are to be evaluated. $\hat{\mathbf{F}}_{i-\frac{1}{2}}$ is known as a vector of effective fluxes. Moreover, expression (78) can be substituted directly into equation (81) to produce the more familiar form of the non-linear advection equation

$$\overline{\mathbf{U}}_i = \frac{\Omega_i^{n\ 1}}{\overline{\Omega}_i} \quad \mathbf{U}_i^{n\ 1} + \frac{\Delta t}{\Omega_i^{n\ 1}} \left[\dot{x}_{i-\frac{1}{2}} \hat{\mathbf{F}}_{i-\frac{1}{2}} - \dot{x}_{i\ \frac{1}{2}} \hat{\mathbf{F}}_{i\ \frac{1}{2}} \right] \Bigg) . \tag{84}$$

From a practical view point the vector equation (81) can be written in

being remapped back to their initial position, equation (12) is made redundant when rezoning is carried out at each time step. A similar observation concerning boundary positions can be made, leaving it unnecessary for the values $x^{n\ \ 1}_{i-\frac{1}{2}}$, $i = 0, 1, \ldots,$ to be calculated and stored.

6 Interface Tracking

The aim of this section is to present in detail a method for improving the resolution of the numerical solution profile at a material interface. The technique, developed b

The Initial Discretisation.

At an initial time $t = t^0$, a material interface is assumed to be located at position x_{ip}, and the computational domain is divided into uniform compututaional cells of size Δx, as detailed in Section 2. If x_{ip} coincides

(c)

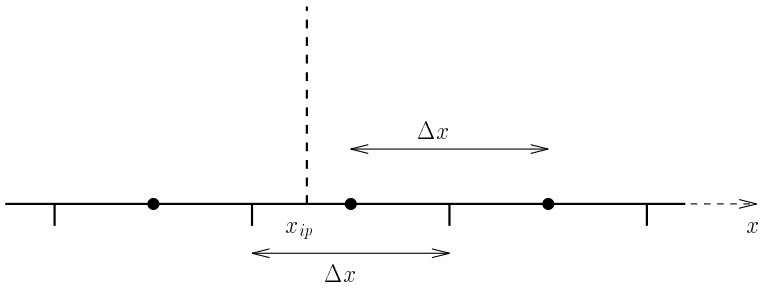
Δx
x_{ip}
x
Δx

( )

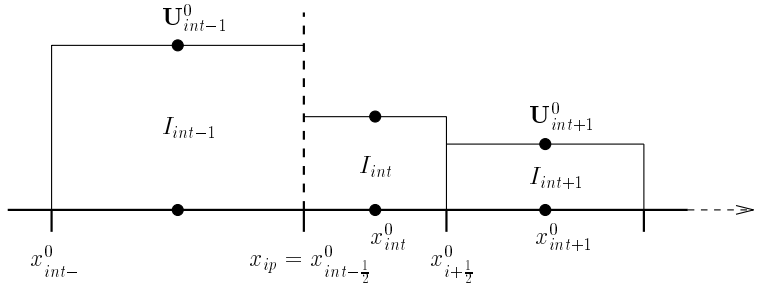
$\mathbf{U}^0_{int-1}$
I_{int-1}
$\mathbf{U}^0_{int+1}$
I_{int}
I_{int+1}
x^0_{int-}
$x_{ip} = x^0_{int-\frac{1}{2}}$
x^0_{int}
$x^0_{i+\frac{1}{2}}$
x^0_{int+1}

boundary which is aligned with the material interface is not remapped. The boundary $x_{int-\frac{1}{2}}$ remains where it was positioned at the end of the Lagrangian

The reconstruction process can be divide into two stages. The first stage is the merging of the non-uniform cell with volume less than $\frac{1}{2}\Delta x$ with its adjacent non-uniform cell. The second stage involves dividing the non-uniform cell with volume greater than $\frac{3}{2}\Delta x$ into a smaller non-uniform cell and a uniform mesh cell. By definition the smaller non-uniform cell will have volume $\Delta\overline{x}_i - \Delta x > \frac{1}{2}\Delta x$

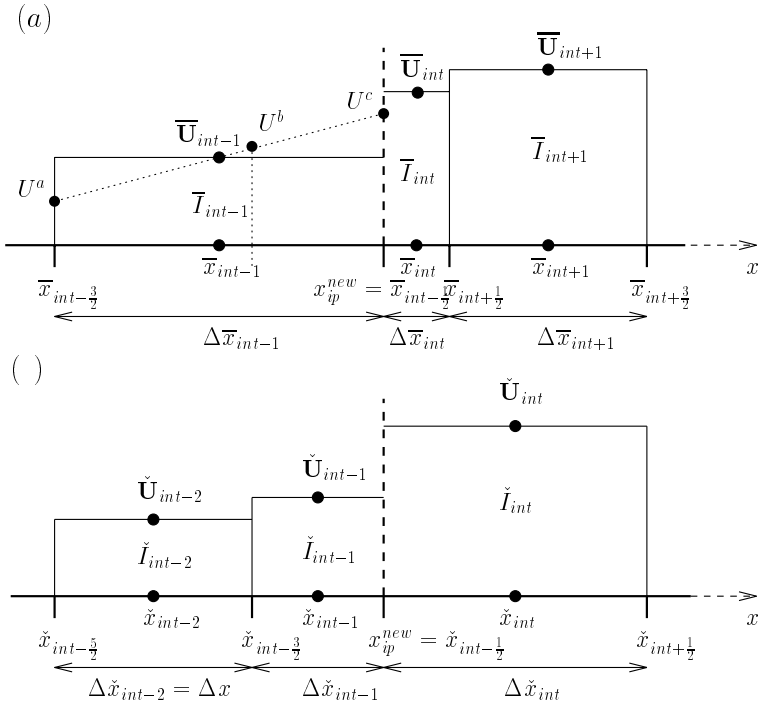

Figure 10: $x - U$ diagram illustrating cell reconstruction for $u_{int-\frac{1}{2}} > 0$.

Cell Division

If the material interface tra

where $\sigma_{int-1-k}$ is a vector of limited first derivative approximations, and k is given by equation (99). The vector $\sigma_{int-1-k}$ is taken to be a function of the vectors $\left(\frac{\overline{\Delta}_{int-\frac{3}{2}-2k}}{\Delta\overline{x}_{int-\frac{3}{2}-2k}} \right)$ and $\left(\frac{\overline{\Delta}_{int-\frac{5}{2}-4k}}{\Delta\overline{x}_{int-\frac{5}{2}-4k}} \right)$, namely

$$\sigma_{int-1-k} = \sigma_{int-1-k} \left(\frac{\overline{\Delta}_{int-\frac{3}{2}-2k}}{\Delta\overline{x}_{int-\frac{3}{2}-2k}}, \frac{\overline{\Delta}_{int\ \ \frac{5}{2}-4k}}{\Delta\overline{x}_{int\ \ \frac{5}{2}-4k}} \right) , \tag{107}$$

where

$$\overline{\Delta}_{int-\frac{3}{2}-2k} = \overline{\mathbf{U}}_{int-1-2k} - \overline{\mathbf{U}}_{int-2-2k} \text{and} \tag{108}$$

$$\overline{\Delta}_{int-\frac{5}{2}}$$

compariative reasons and full details of their implimentation can be found in the book by E. F. Toro [12]. Figures 21 to 29 show the results generated b

the most promising, producing the most accurate solution profile of the three limiters studied. The superiority of the van Leer limiter over the minbee limiter, is also demonstrated.

Lagrangian Methods.

The results from the first-order HLLC and Roe schemes are presented in Figures 21 and 22 respectively. Both figures show equally poor shock resolution, smearing the profile across six cells. The contact discontinuity is captured well by both of the schemes, with the HLLC method exhibiting a slightly sharper resolution. The HLLC results contain an overshoot immediately ahead of the contact dicontinuity, whilst in the Roe results an oscillation is visible directly behind the contact wave. Diffusion of the rarefraction wave, typical of that expected by first-order schemes, is visible in both figures. The Roe scheme achieves greater accuracy at the shock wave than the HLLC scheme.

The results from the second-order HLLC and the Roe schemes are displayed in Figures 23 to 29. Figures 23 to 26 show results for the HLLC method using slope limiters which are 'equivalent' to the flux limiters minbee and superbee. Figures 27 to 29 present the results obtained using the flux limited version of Roe's scheme with the minbee, Van Lem1vsharssuprbeeTalisthatrbm1arefroobc

Lagrange-Remap Methods.

The results from the first-order HLLC and Roe schemes are given in Figures 30 to 33. Figures 30 and 31 are a consequence of applying a piecewise constant remap, whilst Figures 32 and 33 result from using a piecewise linear remap.

The piecewise constant results show no signs of spurious oscillations. There is considerable smearing of discontinuities, most noticable across the contact wave, as highlighted on the density and energy plots. The Roe scheme achieves greater accuracy at the shock wave than the HLLC scheme.

The piecewise linear results demonstrate an expected increase in accuracy over the piecewise constant results. However, spurious oscillations are visible in the figures between the contact and shock waves. These fluctuations are certainly more profound within the Roe results, where there exists a substantial oscillation behind the shock discontinuity.

The results from the second-order HLLC and Roe schemes are displayed in Figures 34 to 47. Figures 34 to 40 present results with a piecewise constant remap, whilst Figures 41 to 47 show results created by applying a piecewise linear remap.

the split HLLC methods show erroneous fluctuations between the shock and contact waves.

For the Roe scheme, limiter-wise it is visible that there is no obvious advantage in adopting either the unsplit or the split approaches when considering accuracy across the shock and rarefraction waves. However, the Lagrange-Remap results are polluted with large spurious oscillations which are not visible in the Eulerian data. Moreover, when considering the results from the Van Leer and superbee limiter, the contact resolution from the split scheme can be viewed as poor when compared to that of the unsplit scheme.

Interface Tracking Method

The results to tests 1 to 3, generated using the second-order HLLC scheme with a piecewise linear interface tracking remap procedure, are displayed in Figures 48 to 53. Figures 48, 50 sultsV

The results from the shock tube problem would seem to suggest that there is no obvious advantage in adopting a Lagrange-Remap approach over an Eulerian method. In fact the data would perhaps prompt the reader to disregard the option of using an split scheme altogether. However, to base a judgement on the results from one test problem alone would be, at best, naive. To make a more informed decision, it would be wise to consider a greater range of test problems in which there were wave interactions and dimensions greater than one.

The split scheme presents the opportunity to consider the solution for the sound wave related transport and the advection related transport separately. It is this authors opinion, that this decomposition offers greater potential for developing an accurate 'fixed grid' solution method, than when faced with the unsplit scenario. Moreover, in this work the results generated using the Lagrangian sc hemes w

higher dimensions. In addition, there is scope for improving or even raising the order of accuracy of the existing Lagrange and Remap phases of the split scheme. For example, Sims [8] explored a piecewise parabolic (third order accurate) remap algorithm.

Alternative methods for accurately resolving a material interface in one and higher dimensions need to be investigated further.

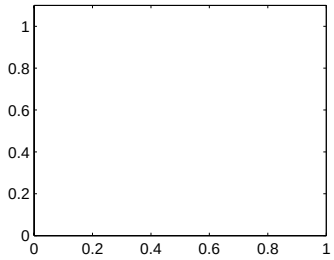
1
0.8
0.6
0.4
0.2
0
0
0.2
0.4
0.6
0.8
1

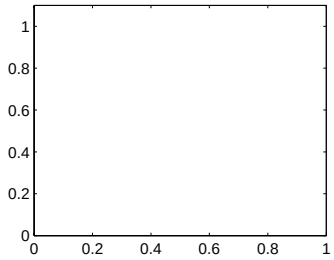
1
0.8
0.6
0.4
0.2
0
0
0.2
0.4
0.6
0.8
1

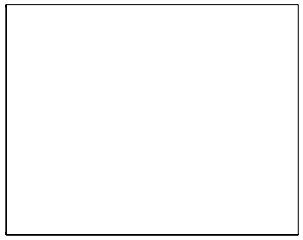
0

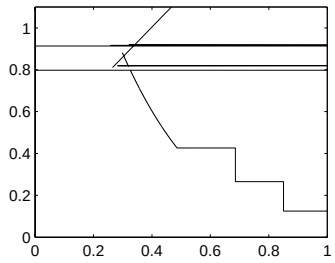
1
0.8
0.6
0.4
0.2
0
0
0.2
0.4
0.6
0.8
1

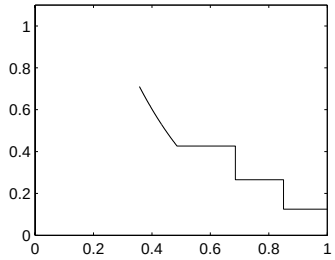
1
0.8
0.6
0.4
0.2
0
0
0.2
0.4
0.6
0.8
1

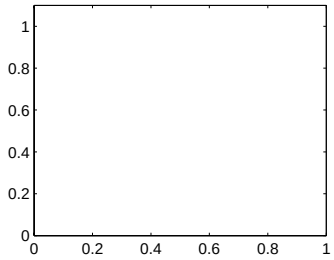
1
0.8
0.6
0.4
0.2
0
0
0.2
0.4
0.6
0.8
1

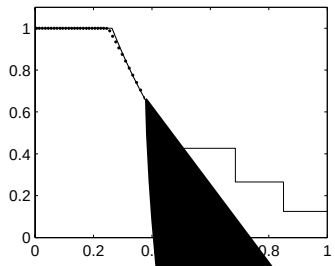
1
0.8
0.6
0.4
0.2
0
0
0.2
0.8
1

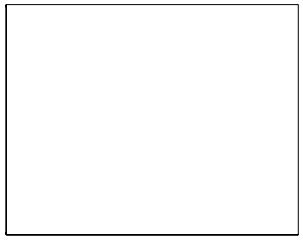
0

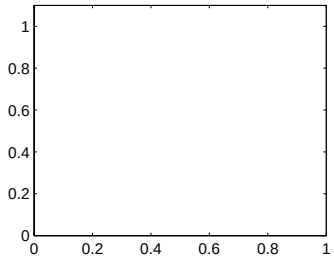
1
0.8
0.6
0.4
0.2
0
0
0.2
0.4
0.6
0.8
1

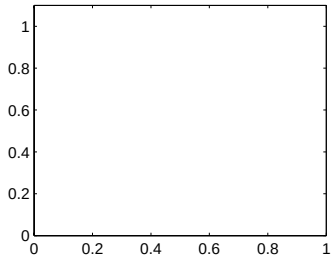
1
0.8
0.6
0.4
0.2
0
0
0.2
0.4
0.6
0.8
1

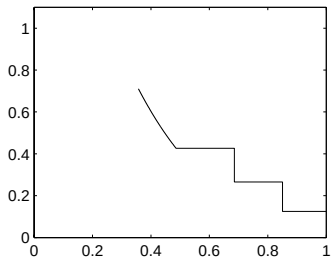
1
0.8
0.6
0.4
0.2
0
0
0.2
0.4
0.6
0.8
1

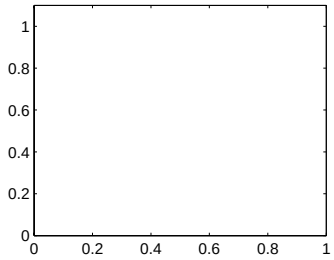
1
0.8
0.6
0.4
0.2
0
0
0.2
0.4
0.6
0.8
1

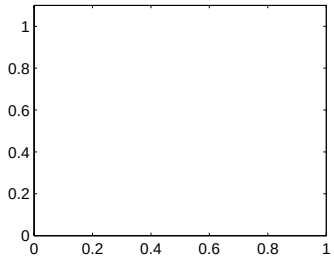
1
0.8
0.6
0.4
0.2
0
0
0.2
0.4
0.6
0.8
1

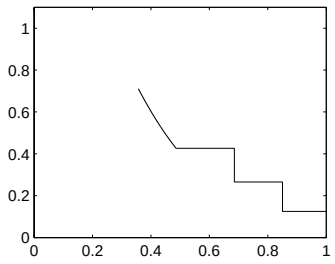
1
0.8
0.6
0.4
0.2
0
0
0.2
0.4
0.6
0.8
1

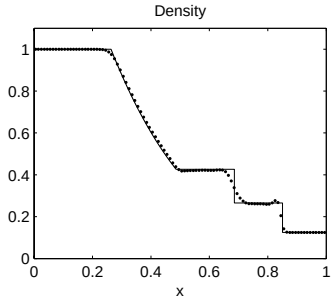
Density
1
0.8
0.6
0.4
0.2
0
0
0.2
0.4
0.6
0.8
1
x

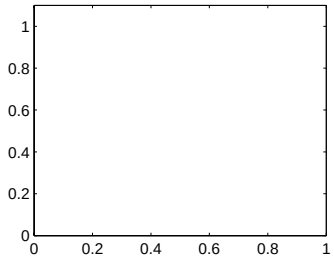
1
0.8
0.6
0.4
0.2
0
0
0.2
0.4
0.6
0.8
1

References

[1] G. Ball. A Free-Lagrange method for unsteady compressible flow: simulation of a confined cylindrical blast wave, Shock Waves, 5 (1996), pp. 311-325.

[2] R. Courant, E. Isaacson, and M. Rees. On the solution of nonlinear hyperbolic differential equation by finite differences, Comm. Pure. Appl. Math. 5 (1952) pp. 243-255.

[3] A. Harten. P. D. Lax, and B. van Leer. On upstream differecing and Godunov-type schemes for hyperbolic conservation laws, SIAM Review, 25(1) (1983) pp. 35-61.

[4] R. J. LeVeque. Numerical methods for conservation laws. Birkhäuser Verlag (1992).

[5] H. Luo, J. D. Baum and R. Löhner. On the computation of multi-material flows using ALE formulation.

[6] W. J. Rider. A review of approximate riemann solvers with godunov's method in lagrangian coordinates, Los Alamos National Laboratory (1994).

[7] P. L. Roe. Approximate Riemann solver, parameter vectors, and difference schemes, Journal of Computational Physics, 43 (1981) pp. 357-372.

[8] P. Sims. Interface tracking using lagrangian-Eulerian methods. PhD Thesis (1990).

[9] G. Sod. A survey of several finite difference methods for systems of nonlinear hyperbolic conservation laws, Journal of Computational Physics, 27 (1978), pp. 1-31.

[10] S. Stokes. Euler Methods with a lagrangian phase in gas dynamics, Msc dissertation, Reading University (1995).

[11] J. Y. Treèpanier, M. Reggio, M. Paraschivoiu and R. Camarero. Unsteady Euler solutions for arbitrarily moving bodies and boundaries, Ameriacan Institute of Aeronautics and Astronautics, 31 (1993) pp. 1869-1876.

[12] E. F. Toro. Riemann solvers and numerical methods for fluid dynamics, Springer-Verlag (1997).

[13] E. F. Toro, M. Spruce, and W.Speares. Restoration of the contact surface in the HLL-Riemann solver. Shock Waves, 4 (1994), pp. 25-34.

[14] B. van Leer. Towards the ultimate conservative difference scheme IV. A new approach to numerical convection, Journal of Computational Physics, 23 (1977) pp. 276-299.

[15] C. D. Munz. On godunov-type schemes for lagrangian gas dynamincs, SIAM Journal of Numerical Analysis, 31 (1994) No. 1, pp. 17-42.

-